Ceramics International 48 (2022) 3070–3080

Contents lists available at ScienceDirect

Ceramics International

journal homepage: www.elsevier.com/locate/ceramint

Enhanced luminescence properties of Li_2MgTiO_4: Mn^{4+}, Ge^{4+} phosphor via single cation substitution for indoor plant cultivation

Sijin Zhang [b,c,1], Shujie Gai [c,d,1], Xiaojuan Zhang [c,d], Mao Xia [b,c], Zhi Zhou [b,c], Xiao Cheng [e], Maohai Yao [f], Maxim S. Molokeev [g,h], Qiuju Feng [a,c,*]

[a] School of Pharmaceutical Sciences, Jishou University, Jishou, 416000, PR China
[b] School of Chemistry and Materials Science, Hunan Agricultural University, Changsha, 410128, PR China
[c] Hunan Provincial Engineering Technology Research Center for Optical Agriculture, Hunan Agricultural University, Changsha, 410128, PR China
[d] College of Bioscience and Biotechnology, Hunan Agricultural University, Changsha, 410128, PR China
[e] Xiangfeng Tea Group Co. Ltd, No. 139 Tianhua North Road, Changsha, Hunan, PR China
[f] Hunan Rare Earth Metal Material Research Institute Co. Ltd, No. 108 Longyuan 2nd Road, Longping High-tech Park, Changsha, Hunan, PR China
[g] Laboratory of Crystal Physics, Kirensky Institute of Physics, Federal Research Center KSC SB RAS, Krasnoyarsk, 660036, Russia
[h] Siberian Federal University, Krasnoyarsk, 660041, Russia

ARTICLE INFO

Keywords:
Mn^{4+}
Titanate
Cationic substitution
Indoor plant cultivation

ABSTRACT

Red and far-red emitting phosphors have been widely used in phosphor-converted light emitting diode (pc-LED) devices to provide lighting for indoor plant growth, thus achieving desired product qualities. Among the many ways to optimize phosphors' optical performance, cationic substitution is one of the most effective methods. In this study, red phosphors ($Li_2MgTi_{1-x-y}O_4$: xMn^{4+}, yGe^{4+}) were synthesized by high temperature solid state method and the optical performance of phosphors were improved with increasing Ge^{4+} constituents. In particular, luminescence intensity of Li_2MgTiO_4: $0.002Mn^{4+}$, $0.1Ge^{4+}$ increased by 152% under 468 nm excitation, and the thermostability of emission intensity increases from 22% ($y = 0$) to 43% ($y = 0.1$), which is about twice as much. Finally, pc-LED device was fabricated via the red phosphor Li_2MgTiO_4: $0.002Mn^{4+}$,$0.1Ge^{4+}$ coated on a 470 nm ultraviolet chip. By changing the proportion of the phosphor, the electroluminescence spectra of pc-LED device could match well with the absorption regions of plant pigments. Therefore, Li_2MgTiO_4: $0.002Mn^{4+}$, $0.1Ge^{4+}$ phosphor has potential application in plant lighting. Furthermore, this work can offer some helpful references for improving luminescent efficiency by simply modulating the chemical composition.

1. Introduction

Light is a significant environmental factor for regulating plant photosynthesis, substance metabolism and gene expression [1–3]. According to the absorption spectra of plant pigments, Carotenoids Chlorophyll A and B absorb 450 nm blue light and 660 nm red light, while phytochrome P_R and P_{FR} absorb 660 nm red and 730 nm far-red light [4–6]. In the past, plant lighting used traditional light sources such as incandescent lamp, low pressure gas discharge fluorescent lamp, high pressure gas discharge lamp such as high pressure sodium lamp and high pressure metal halide lamp and so on. However, the wavelength range of the traditional plant growth lighting sources do not exactly match the absorption spectrum of the plant, and these devices generally have short life spans and are not economically sustainable [7,8]. Nowadays, pc-LED devices make it possible to supplement light to plants, regulate plant morphology, photosynthesis, blossom and bear fruit because of their huge advantages in dimming method and spectral modulation. Pc-LED devices possess the advantages of energy saving, high photoelectric conversion efficiency, long luminescent life, non-toxic and harmless, in addition, they can better match the absorption spectrum of plant pigments [9,10]. Therefore, pc-LED devices play an important constructive role in indoor plant lighting, improving quality of agricultural products and potentially generating more revenue [11].

At present, there are two main assembly types of pc-LED plant growth lamps: one is to coat red and far-red phosphors on the blue chips, and the other is to combine near ultraviolet chips with blue, red and far

* Corresponding author. School of Pharmaceutical Sciences, Jishou University, Jishou, 416000, PR China.
E-mail address: Fqj245@126.com (Q. Feng).
[1] Sijin Zhang and Shujie Gai contributed equally to this work.

https://doi.org/10.1016/j.ceramint.2021.10.082
Received 10 August 2021; Received in revised form 13 October 2021; Accepted 14 October 2021
Available online 15 October 2021
0272-8842/© 2021 Elsevier Ltd and Techna Group S.r.l. All rights reserved.

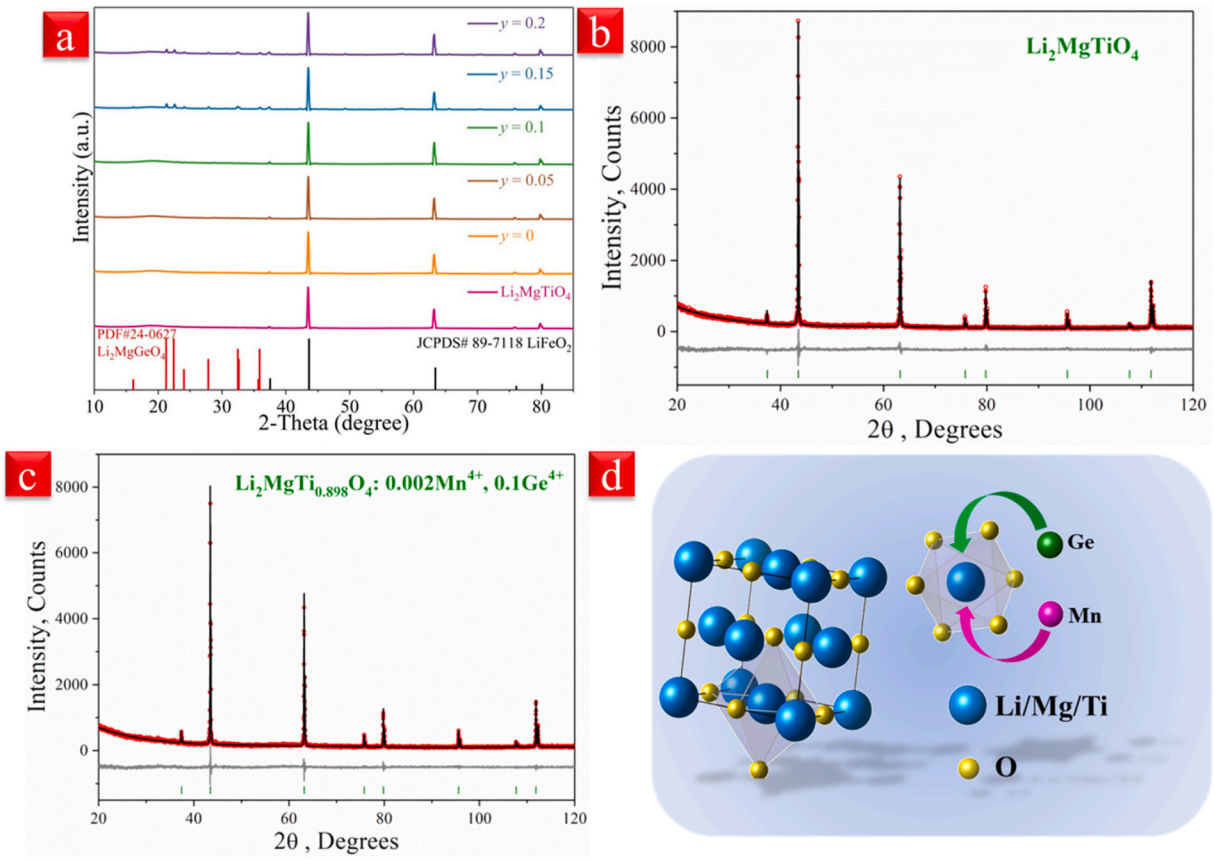

Fig. 1. (a) XRD patterns of Li_2MgTiO_4 host and $Li_2MgTi_{0.998-y}O_4$: $0.002Mn^{4+}$, yGe^{4+} phosphors. (b), (c) Rietveld refinement patterns of $Li_2MgTi_{0.998}O_4$: $0.002Mn^{4+}$ and $Li_2MgTi_{0.898}O_4$: $0.002Mn^{4+}$, $0.1Ge^{4+}$. (d) The crystal structure of Li_2MgTiO_4 host and the substitution mechanism of Mn^{4+} and Ge^{4+} ions.

red phosphors [12]. Commercial phosphor $Y_3Al_5O_{12}:Ce^{3+}$ is not suitable for plant lighting application because its spectrum does not match the absorption spectrum of plants. and it is mainly used for white light-emitting diodes (WLEDs) [13,14]. Eu^{2+} doped nitride phosphors such as $CaAlSiN_3$: Eu^{2+}, $SrAlSiN_3$: Eu^{2+} [15,16], $Ca_2Si_5N_8$: Eu^{2+} and $Sr_2Si_5N_8$: Eu^{2+} [17,18] have limited application in agriculture due to their difficult synthesis and high cost. Such fluoride phosphors including K_2TiF_6: Mn^{4+} and K_2SiF_6: Mn^{4+} and so on, which have not been widely used in plant lighting because of the adverse environmental effects caused by the use of hydrofluoric acid in the synthesis process [19,20]. Therefore, extensive efforts have focused mainly on the development of spectral matching, cheap and environment friendly phosphors to avoid these weaknesses.

In addition, numerous excellent phosphors that can be used for plant lighting by cationic substitution have been reported in recent years. For example, Zheng et al. [21] substituted Ca^{2+} and Al^{3+} with Y^{3+} and Mg^{2+} in $CaAl_{12}O_{19}$: Mn^{4+} phosphor, which enhanced the luminescence intensity of Mn^{4+} and obtained tunable red and far red light. Fang et al. [22] formed defective energy levels in the crystal lattice through Ca^{2+} doping, which enabled the $LaAlO_3$: Mn^{4+} phosphor to achieve a zero thermal quenching performance. Gu et al. [23] synthesized $SrMgAl_{10-y}Ga_yO_{17}$: Mn^{4+} phosphors by replacing Al^{3+} with Ga^{3+}. From the report, it can be clearly observed that the spectral redshift tunable luminescence and the luminescence intensity enhancement.

A cheap and easy to synthesize phosphor Li_2MgTiO_4: Mn^{4+} has been reported, whose photoluminescence (PL) spectra matched well with the absorption spectra of plant pigments [24]. However, its poor thermal stability and low quantum yield limit its application. In view of the problem, Nien et al. [25] improved the luminescent performance of the Li_2MgTiO_4: Mn^{4+} phosphor by replacing Ti^{4+} with Hf^{4+}, but the thermal stability and internal quantum yield did not show significant improvement. Herein, we reported that a series of phosphors $Li_2MgTi_{1-x-y}O_4$: xMn^{4+}, yGe^{4+}. The fluorescence properties, especially the luminescence intensity and thermal stability, were greatly improved by modification. It is clear that the electroluminescence (EL) spectra of fabricated pc-LED were well matched with the absorption spectrum of plant pigment, which indicates that the phosphor has the potential to be used in indoor plant lighting. The phase structure, PL spectra, internal quantum yield (IQY), luminescence lifetime and EL spectra of the phosphor were studied in detail.

2. Experimental section

2.1. Materials and synthesis

A series of $Li_2MgTi_{1-x}O_4$: xMn^{4+} ($x = 0$, 0.001, 0.002, 0.003, 0.004, 0.005) and $Li_2MgTi_{0.998-y}O_4$: $0.002Mn^{4+}$, yGe^{4+} ($y = 0$, 0.05, 0.1, 0.15, 0.2) phosphors were synthesized by high temperature solid state method. The raw materials were picked out and bought from Macklin and Aladdin, which were weighed according to stoichiometric ratios including Li_2CO_3 (99.99%), MgO (99%), TiO_2 (99%), and MnO_2 (99%). The mixtures were thoroughly ground for 30 min with an appropriate amount of ethanol as dispersant. Then they were pre-heated at 600 °C for 6 h, 1000 °C for 2 h, and then cooled naturally. The reactants, which

Table 1
Main parameters of processing and refinement of the Li_2MgTiO_4: xMn^{4+}, yGe^{4+} samples.

x, y	Space Group	Cell parameters (Å), Cell Volume (Å^3)	R_{wp}, R_p, R_B, χ^2
0, 0	*Fm-3m*	$a = 4.15869$ (4), $V = 71.924$ (2)	8.84, 6.82, 2.19, 1.28
0.002, 0.1	*Fm-3m*	$a = 4.15765$ (3), $V = 71.8695$ (15)	8.74, 6.79, 0.87, 1.27

were further ground for 10 min, were sintered at 1300 °C and held for 2 h. Finally, the samples were cooled down to RT and ground again for subsequent characterization analysis.

2.2. Characterization

The X-ray diffraction (XRD) detection range of the sample was set to 10–85° by a diffractometer (PANalytical, Netherlands). The powder diffraction data of Li_2MgTiO_4: *x*Mn, *y*Ge ($x = 0$, 0.002; $y = 0$, 0.1) for Rietveld analysis were collected at room temperature with a Bruker D8 ADVANCE powder diffractometer (Cu-Kα radiation) and linear VANTEC detector. The step size of 2θ was 0.02°, and the counting time was 2 s per step. The microstructure of the samples were investigated using an ultrahigh resolution field emission scanning electron microscopy (Tescan Clara, Czech). The photoluminescence spectra were detected by a fluorescence spectrophotometer (F-4700, Hitachi, Japan) equipped with a 150 W Xe lamp. The thermal resistance was tested via placing a thermal control device (Orient KOJI, China) in the above fluorescence spectrophotometer. Fluorescence lifetime was obtained by a spectrometer (FLS 920, Edinburgh, UK), equipped with a microsecond pulsed Xe lamps. UV–vis absorption spectra were collected by using a spectrophotometer (U-4100, Hitachi, Japan). The internal quantum yield was obtained by QE-2100 measurement system (Otsuka, Japan). The ATA-500 (Everfine, China) analysis system was used for measuring the EL spectra of LED devices. All of the above tests were performed at room temperature except for the thermal resistance test.

3. Result and discussion

3.1. Phase morphology

Fig. 1a exhibits XRD patterns of the Li_2MgTiO_4 host and $Li_2MgTi_{0.998-y}O_4$: $0.002Mn^{4+}$, yGe^{4+} ($y = 0$, 0.05, 0.10, 0.15, 0.2). Due to the lack of crystal structure data of Li_2MgTiO_4 in the database, the standard card of $LiFeO_2$ (JCPDS# 89–7118) with similar structure was used for comparison. The XRD patterns indicate that the ionic modifications have little effect on the phase structure when the concentration is less than 0.1. The presence of a higher concentration of Ge^{4+} seems to lead to the development of a second phase, which matches well with the part of Li_2MgGeO_4 standard card (PDF# 24–0627). To obtain the detailed

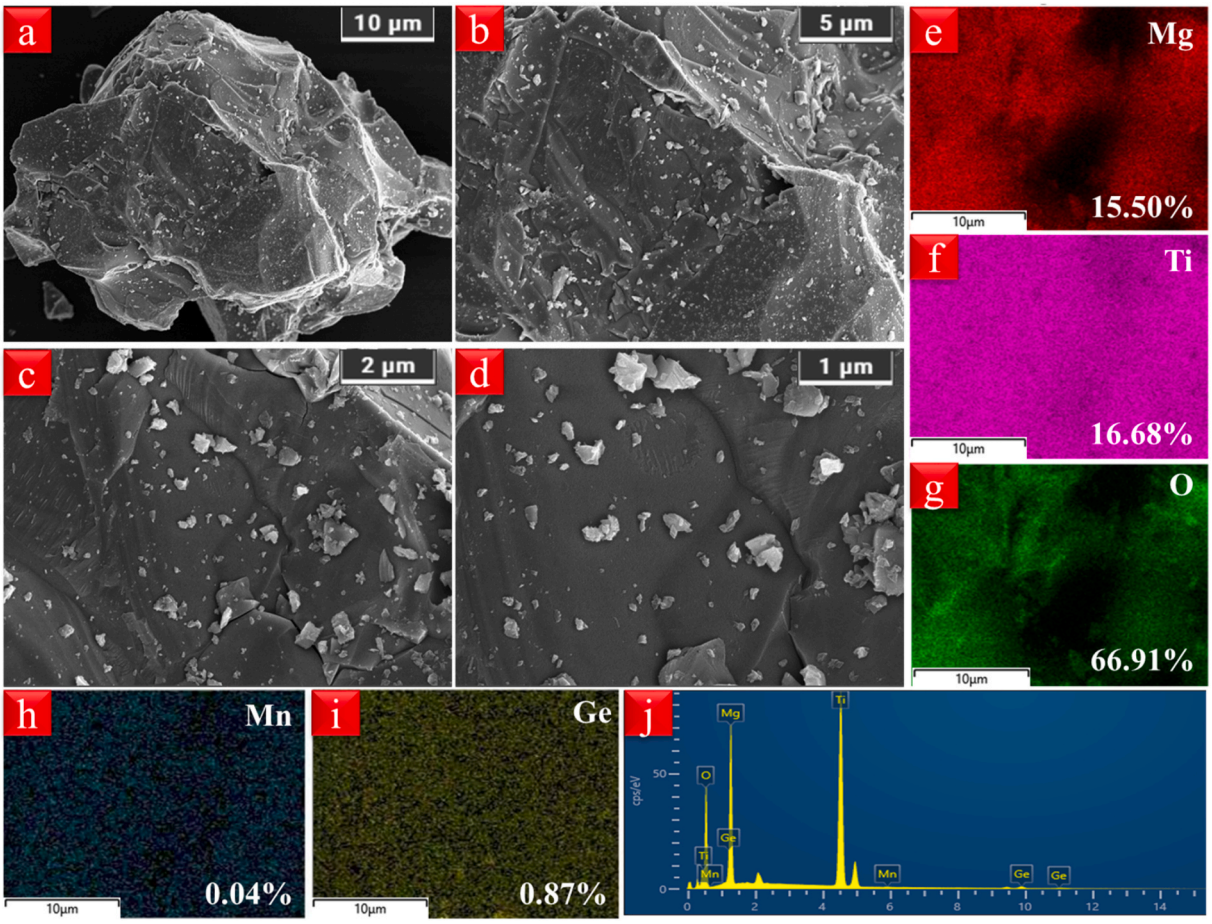

Fig. 2. (a–d) SEM images of $Li_2MgTi_{0.898}O_4$: $0.002Mn^{4+}$, $0.1Ge^{4+}$ phosphor with various detecting scales. (f–j) Elemental maps of characteristic particle of $Li_2MgTi_{0.898}O_4$: $0.002Mn^{4+}$, $0.1Ge^{4+}$ phosphor.

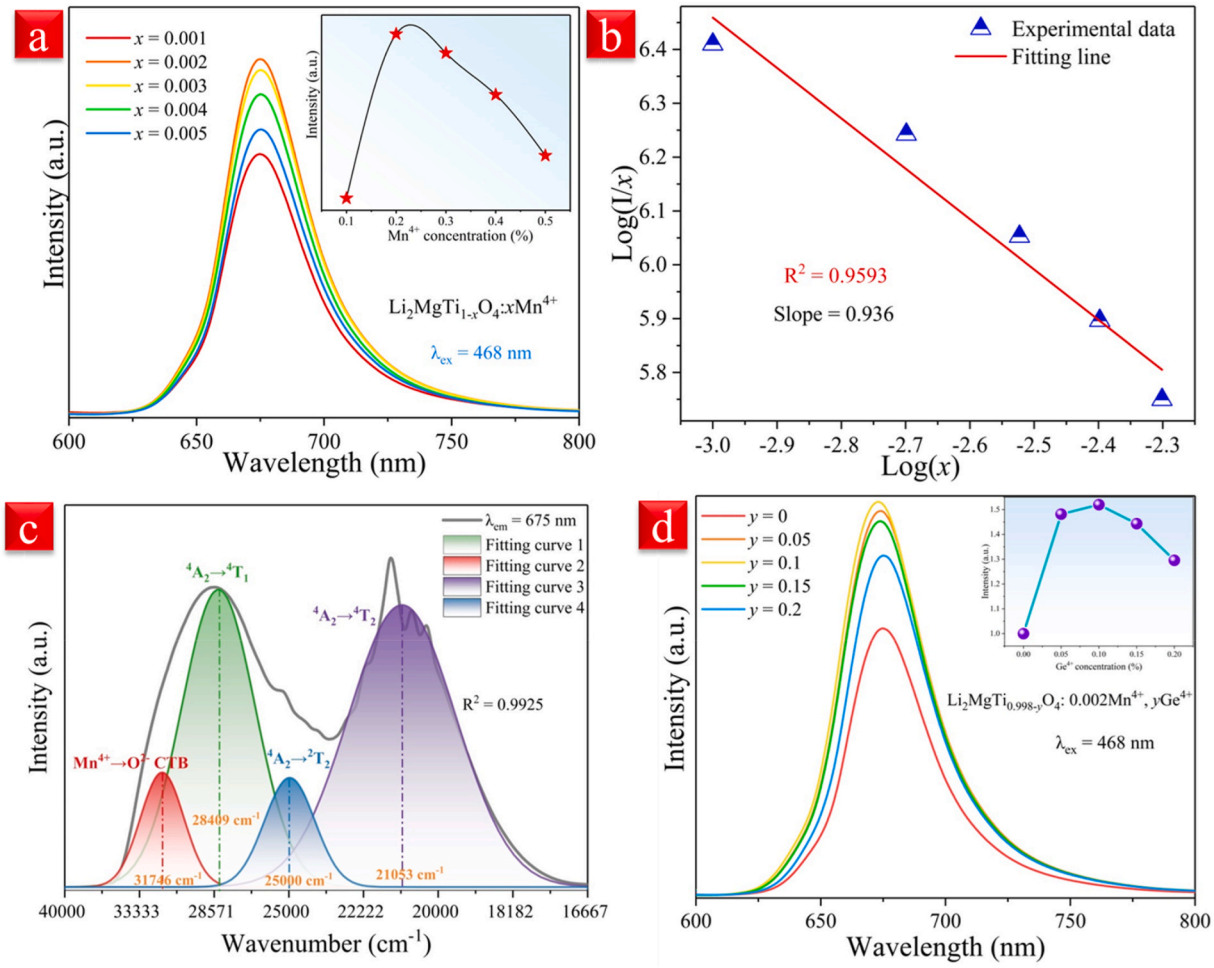

Fig. 3. (a) PL spectra of $Li_2MgTi_{1-x}O_4$: xMn^{4+}, the inset is the relationship between Mn^{4+} concentration and luminescence intensity. (b) The relationship between log (x) and log(I/x). (c) PLE spectra and Multi-peaks Gaussian fitting of $Li_2MgTi_{0.998}O_4$: $0.002Mn^{4+}$. (d) PL and PLE spectra of $Li_2MgTi_{0.998-y}O_4$: $0.002Mn^{4+}$, yGe^{4+}, the inset is the tendency of emission intensity.

crystal structure data of the samples, Rietveld refinement was performed using TOPAS 4.2 as shown in Fig. 1b and c. The refined results were stable and gave low R-factors which are listed in Table 1. The crystal structure (Fig. 1d) shows that the Li, Mg and Ti atoms are all coordinated with six oxygen atoms to form an octahedron with space group Fm3m. According to the effective radius theory, the effective ionic radius of Mn^{4+} (0.53 Å, CN = 6) and Ge^{4+} (0.53 Å, CN = 6) are close to those of Ti^{4+} (0.605 Å, CN = 6), while different from that of Li^{+} (0.76 Å, CN = 6) and Mg^{2+} (0.72 Å, CN = 6). For another, Mn^{4+}, Ge^{4+} and Ti^{4+} ions have equal valance. So to wrap up here, Mn^{4+} and Ge^{4+} ions preferably substituted Ti^{4+} at octahedral sites, which also confirms the reduction in cell volume.

In order to further explore the morphology and chemical composition of the $Li_2MgTi_{0.898}O_4$: $0.002Mn^{4+}$, $0.1Ge^{4+}$ phosphor, it was tested by scanning electron microscopy. Fig. 2a–d are the SEM images of the phosphor at different magnification. The particles are condensed and irregularly shaped, similar to most phosphors synthesized by high temperature solid state method. The average grain diameter is about 120–130 μm. In addition, the energy dispersive spectrum (EDS) analysis as shown in Fig. 2e–j indicates that the elements are evenly distributed in the particle. However, the EDS mapping of Li cannot be detected because the energy of Li is too small. These results indicate that $Li_2MgTi_{0.898}O_4$: $0.002Mn^{4+}$, $0.1Ge^{4+}$ phosphors were synthesized successfully by high temperature solid state method.

3.2. Luminescence properties

Fig. 3a presents the PL spectra of $Li_2MgTi_{1-x}O_4$: xMn^{4+} (x = 0.001–0.005). It can be seen from the spectra that the luminescence intensity is a function of Mn^{4+} concentration, reaching maximum when the concentration is 0.002. This phenomenon is caused by the concentration quenching effect, which can be confirmed by calculating the critical distance (R_c) between Mn^{4+}. When the distance of Mn^{4+}-Mn^{4+} is less than 5 Å, the exchange interaction is effective, otherwise interaction is mostly multipolar and invalid. The R_c is defined by equation (1) [26]:

$$R_c \approx 2\left(\frac{3V}{4\pi x_c N}\right)^{\frac{1}{3}} \quad (1)$$

herein, V is the cell volume, x_c refers to the critical concentration of Mn^{4+}, and N stands for the number of sites that Mn^{4+} could occupy.

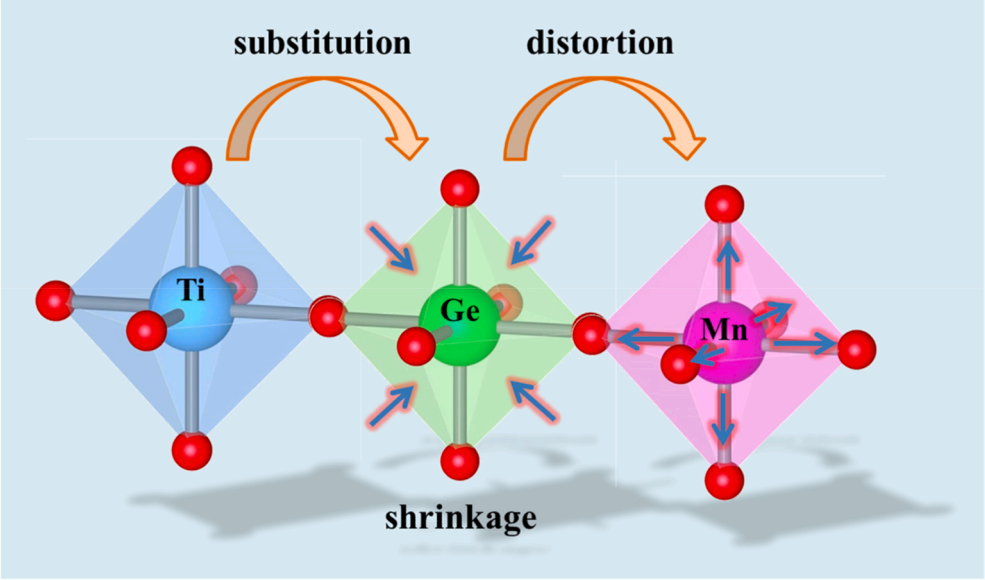

Fig. 4. The mechanism of red emission enhancement. (For interpretation of the references to colour in this figure legend, the reader is referred to the Web version of this article.)

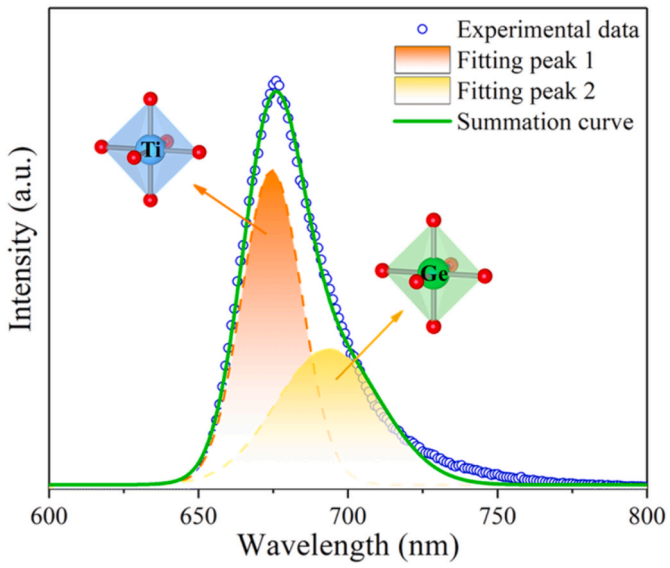

Fig. 5. Emission spectrum of $Li_2MgTi_{0.898}O_4$: $0.002Mn^{4+}$, $0.1Ge^{4+}$ under 468 nm excitation at 5 K and the Gaussian peaks fitting.

From $V = 71.27$ Å^3, $x_c = 0.002$, $N = 1$ and the above equation, the value of R_c is calculated to be 20.42 Å. Because R_c is greater than 5 Å, the concentration quenching of $Li_2MgTi_{1-x}O_4$: xMn^{4+} can be attributable to the multipolar-multipolar interaction, split into exchange interaction, dipole-dipole (d-d), dipole-quadrupole (d-q), and quadrupole-quadrupole (q-q) interactions, respectively. Dexter's theory can be used to explain the interactions [27]:

$$\frac{I}{x} = k\left[1 + \beta(x)^{\frac{\theta}{3}}\right]^{-1} \quad (2)$$

herein, k and β represent the certain excitation condition and specific matrix crystal, I stand for the luminescence intensity, x is the concentration of Mn^{4+}, and θ could be equal to 3 (exchange interaction), 6 (d-d), 8 (d-q), 10 (q-q) Fig. 3b exhibits a linear fitting of the relationship between log (x) and log (I/x). The slope of fitting curve is −0.936. Then the θ is calculated to be 2.808, which is close to 3. This value reveals that the concentration quenching mechanism of the phosphor is the exchange interaction between the nearest neighboring ions in this work.

The PLE spectra of $Li_2MgTi_{0.998}O_4$: $0.002Mn^{4+}$ was measured at 675 nm, and then the deconvolution PLE spectrum was obtained by Gaussian analysis, as presented in Fig. 3c. The PLE spectrum can be divided into four bands located at, 31746 cm^{-1}, 28409 cm^{-1}, 25000 cm^{-1} and 21053 cm^{-1}. The peak at 31746 cm^{-1} is originated from the Mn^{4+}-O^{2-} charge transfer band, and the peak at 28409 cm^{-1}, 25000 cm^{-1} and 21053 cm^{-1} is attributed to $^4A_2 \rightarrow {}^4T_1$, $^4A_2 \rightarrow {}^2T_2$ and $^4A_2 \rightarrow {}^4T_2$ spin-allowed transitions of Mn^{4+}, respectively. The PLE spectrum shows a wide band from 250 nm to 600 nm. Most notably, the strong peaks locked at 348 nm and 468 nm, which indicates that the phosphor can be excited by ultraviolet or blue chip. Fig. 3d exhibits the variation of PL and PLE spectra with Ge^{4+} concentration. With the increase of Ge^{4+} concentration from 0 to 0.2, the emission intensity of the phosphor increases and then decreases, which reaches the maximum value when the concentration is 0.1, increasing by 152%.

In the Mn^{4+} doped phosphors, the interaction between Mn^{4+} influences the luminescence intensity, while the isolated Mn^{4+} is favorable for luminescence. Although the increase of Mn^{4+} concentration leads to the enhancement of luminescence intensity, the concentration quenching will inhibit the further improvement of luminescence intensity when Mn^{4+} exceeds a certain concentration. Fig. 4 shows the mechanism of red emission enhancement. In the absence of Ge^{4+}, Mn^{4+} replaces Ti^{4+} sites to form O^{2-}-Ti^{4+}-O^{2-}-Mn^{4+}-O^{2-} pairs. In the presence of Ge^{4+}, the lattice around Mn^{4+} can be modulated by Ge^{4+} to form O^{2-}-Ge^{4+}-O^{2-}-Mn^{4+}-O^{2-} pairs, which increases the number of isolated Mn^{4+} [28]. Meanwhile, increasing the Mn^{4+}-Mn^{4+} distance can weaken the Mn^{4+} orbital hybridization and improve the Mn^{4+} emission energy [29]. The [MnO_6] octahedral lattice distortion and the distance between Mn^{4+}

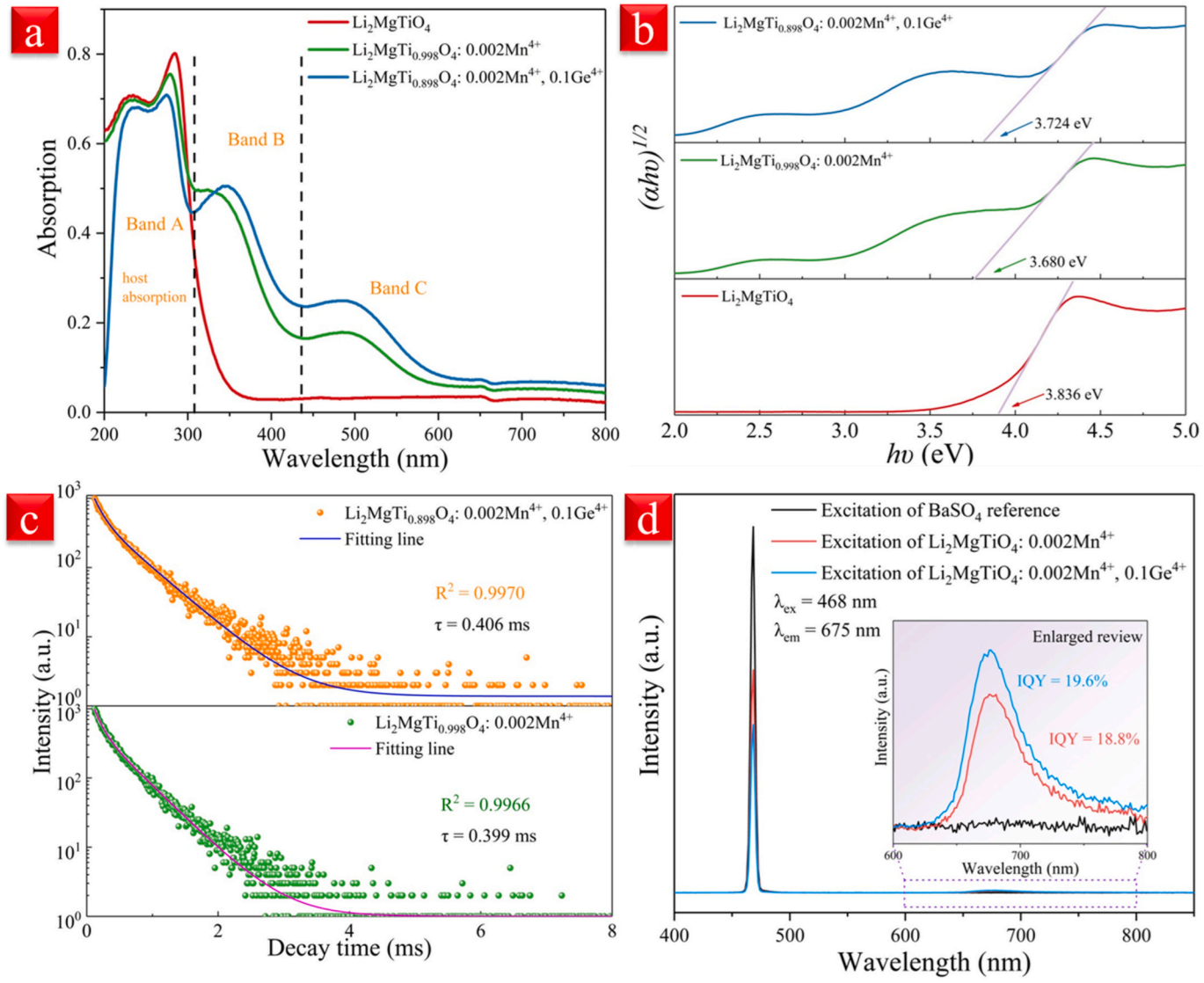

Fig. 6. (a) UV–vis absorption spectra of the Li_2MgTiO_4 host, $Li_2MgTi_{0.998}O_4$: $0.002Mn^{4+}$ and $Li_2MgTi_{0.898}O_4$: $0.002Mn^{4+}$, $0.1Ge^{4+}$. (b) The fitting band gap value. (c) Decay curves of the $Li_2MgTi_{0.898}O_4$: $0.002Mn^{4+}$, $0.1Ge^{4+}$ and $Li_2MgTi_{0.998}O_4$: $0.002Mn^{4+}$ (d) The internal quantum yield of the $Li_2MgTi_{0.998}O_4$: $0.002Mn^{4+}$ and $Li_2MgTi_{0.898}O_4$: $0.002Mn^{4+}$, $0.1Ge^{4+}$ phosphors.

increased due to the lattice shrinks after Ge^{4+} replaces Ti^{4+}, which also reduces the probability of forming quenching center and decreases energy transfer probability between Mn^{4+}. Therefore, [MnO_6] octahedron can be converted into distorted via replacing Ti^{4+} with Ge^{4+} thus improving luminescence intensity and efficiency. When the Ge^{4+} concentration is greater than 0.1, the emission intensity starts to reduce on account of the formation of second phase Li_2MgGeO_4. This phenomenon is consistent with the XRD patterns and its luminescence properties of doped Mn^{4+} has been reported [30]. In addition, with the increase of Ge^{4+} concentration, [GeO_6] and [TiO_6] sites will be formed, and Mn^{4+} will tend to replace these two sites. To prove this, the emission spectra at low temperature (5 K) was measured as shown in Fig. 5, which could be divided into two peaks at 674 nm and 693 nm by the Gaussian fitting. Then combine the following equation to explain the phenomenon [31]:

$$D_q = \frac{1}{6} Ze^2 \frac{r^4}{R^5} \tag{3}$$

where Z stand for the charge of the anion, e is electron charge, r refer to the radius of the d wave function, and R represents the bond length. In general, the smaller the D_q is, the shorter the emission wavelength will be. According to the different radii of Ge^{4+} and Ti^{4+}, it can be inferred that the peaks of 674 nm and 693 nm are attributed to the sites where Ti^{4+} and Ge^{4+} are replaced by Mn^{4+}, respectively.

The UV–vis absorption spectra of Li_2MgTiO_4, $Li_2MgTi_{0.998}O_4$: $0.002Mn^{4+}$ and $Li_2MgTi_{0.898}O_4$: $0.002Mn^{4+}$, $0.1Ge^{4+}$ are shown in Fig. 6a, which can be found that no obvious intrinsic absorptions in 200–800 nm for Li_2MgTiO_4, but the phosphor compounds start adsorbing 200–800 nm wavelength after the doping of Mn^{4+} and Ge^{4+}, with higher absorption intensity from samples doped with Ge^{4+} than Mn^{4+}. Their absorption spectra can be divided into three absorption bands, namely band A, band B, and band C. These three bands correspond to the host absorption of Mn^{4+} and the energy level transition of $^4A_2 \rightarrow {}^4T_1$, $^4A_2 \rightarrow {}^2T_2$ and $^4A_2 \rightarrow {}^4T_2$ respectively, which keep consistence with the Gaussian fitting of the excitation spectra above. Then the band

gap energy of these samples can be obtained by the following equation [32,33]:

$$(\alpha h\upsilon)^n = A\left(h\upsilon - E_g\right) \tag{4}$$

where α, $h\upsilon$, A, and E_g represent the absorption parameter, proportional constant, photon energy and the band gap, respectively. Fig. 6b shows that the bandgap energies of Li_2MgTiO_4, $Li_2MgTi_{0.998}O_4$: $0.002Mn^{4+}$ and $Li_2MgTi_{0.898}O_4$: $0.002Mn^{4+}$, $0.1Ge^{4+}$ are 3.836 eV, 3.680 eV, and 3.724 eV, respectively, indicating that the introduction of Mn^{4+} and Ge^{4+} could lead to the change of E_g.

The luminescence lifetime of $Li_2MgTi_{0.898}O_4$: $0.002Mn^{4+}$, $0.1Ge^{4+}$ and $Li_2MgTi_{0.998}O_4$: $0.002Mn^{4+}$ were measured, as shown in Fig. 6c, which can be well fitted by the double-exponential decay model. This model and the average lifetime $\tau_{ave.}$ are shown as follows [34,35]:

$$I(t) = I_0 + M\exp\left(-\frac{t}{\tau_1}\right) + N\exp\left(-\frac{t}{\tau_2}\right) \tag{5}$$

$$\tau_{ave} = \frac{\left(c_1\tau_1^2 + c_2\tau_2^2\right)}{\left(c_1\tau_1 + c_2\tau_2\right)} \tag{6}$$

herein, $I(t)$ and I_0 refer to the luminescence intensities at time t and 0, M and N stand for a constant, τ_1 and τ_2 represent the exponential component of decay time, c_1 and c_2 stand for the pre-exponential factors respectively. The average lifetime $\tau_{ave.}$ of the two samples were calculated to be 0.406 ms and 0.399 ms.

The internal quantum yield (IQY), an important parameter for evaluating the photoelectric conversion ability of optoelectronic devices, is showed in Fig. 6d and can be determined via following formula [36,37]:

$$\eta = \frac{\int L_S}{\int E_R - \int E_S} \tag{7}$$

where L_S is the emission spectra of the phosphor, E_R and E_S refer to the excitation curve with $BaSO_4$ and the phosphor, η stand for the internal quantum yield. The IQY of $Li_2MgTi_{0.998}O_4$: $0.002Mn^{4+}$ and $Li_2MgTi_{0.898}O_4$: $0.002Mn^{4+}$, $0.1Ge^{4+}$ phosphors are calculated to be 18.8% and 19.6%, respectively. For practical application, the IQY must be further enhanced.

The combination of Tanabe–Sugano energy level diagram [38] and the luminescence mechanism diagram, as shown in Fig. 7, can reveal the luminescence mechanism of phosphor well. The blue light (468 nm) excites electrons of Mn^{4+} to transition from $^4A_2$–$^4T_2$, $^2T_2$ and $^4T_1$. Then the excited state electrons are relaxed to the lowest excited state energy level by a non-radiative transition, and then return to the ground state emitting red light at 675 nm, resulting in the spin-forbidden $^2E \rightarrow {}^4A_2$ transition. The crystal field intensity can be calculated by formula (8):

$$D_q = \frac{E\left({}^4A_2 - {}^4T_2\right)}{10} \tag{8}$$

The Racah parameter B can be defined as formula (9):

$$\frac{D_q}{B} = \frac{15(x-8)}{x^2 - 10x} \tag{9}$$

The parameter x can be got from formula (10):

$$x = \frac{E\left({}^4A_2 - {}^4T_1\right) - E\left({}^4A_2 - {}^4T_2\right)}{D_q} \tag{10}$$

According to the peak energy of the level transition $^2E \rightarrow {}^4A_2$ and the above parameters, C can be obtained from formula (11):

$$\frac{E\left({}^2E - {}^4A_2\right)}{B} = \frac{3.05C}{B} + 7.9 - \frac{1.8B}{D_q} \tag{11}$$

To sum up, the values of B, C, D_q, and D_q/B are calculated to be 708 cm^{-1}, 3164 cm^{-1}, 2105 cm^{-1}, and 2.97. The D_q/B is greater than 2.2, indicating that Mn^{4+} ions exist in a strong crystal field in the Li_2MgTiO_4 host [39,40]. The energy states and crystal field parameters in $Li_2MgTi_{0.998-y}O_4$: $0.002Mn^{4+}$, yGe^{4+} are shown in Table 2. The intensity of the

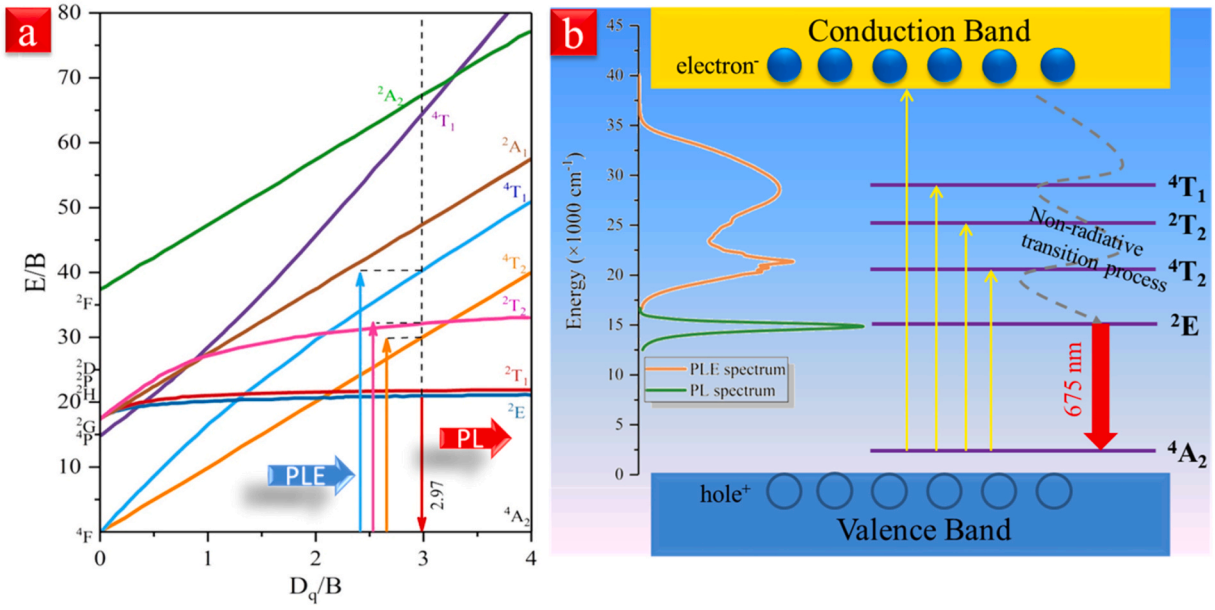

Fig. 7. (a) The Tanabe-Sugano energy level diagram for d^3 electron configuration (Mn^{4+}) in octahedron symmetry. (b) Mechanism diagram of luminescence in $Li_2MgTi_{1-x-y}O_4$: xMn^{4+}, yGe^{4+} phosphors.

Table 2
Energy states and crystal field parameters in $Li_2MgTi_{0.998}O_4$: $0.002Mn^{4+}$ and $Li_2MgTi_{0.898}O_4$: $0.002Mn^{4+}$, yGe^{4+} phosphors.

y	E ($^4A_2$–$^4T_1$)	E ($^4A_2$–$^4T_2$)	E (^2E–$^4A_2$)	D_q	B	C	D_q/B
0	28409	21053	14815	2105	708	3164	2.97
0.05	28490	21413	14792	2141	673	3231	3.18
0.1	28653	21505	14815	2151	680	3223	3.16
0.15	28409	21413	14815	2141	665	3257	3.22
0.2	28169	21142	14792	2114	667	3246	3.17

crystal field changed slightly before and after doping, which also confirmed that the emission spectrum had a 1–2 nm peak shift.

3.3. Thermal resistance

The thermal resistance of phosphors is an important factor to evaluate LED devices. When the devices are used, the central temperature can reach about 150 °C, and the higher thermal resistance will lead to longer device lifetime. Equation (12) was used to calculate the thermal resistance (TR) of the phosphors at different temperature [38]:

$$TR = \frac{\int_b^a I_T(x)dx}{\int_b^a I_0(x)dx} * 100\% \quad (12)$$

herein, I_T represent the luminescence intensity at test temperature and I_0 is the luminescence intensity at room temperature. As shown in Fig. 8, without Ge^{4+} doping, the thermal resistance of the $Li_2MgTi_{0.998}O_4$: $0.002Mn^{4+}$ phosphor at 150 °C is 21.7%, which is a relatively low value, possibly due to the instability of the material lattice. When doped with Ge^{4+}, the thermal resistance of the $Li_2MgTi_{0.898}O_4$: $0.002Mn^{4+}$, $0.1Ge^{4+}$ reached 42.9% at 150 °C, almost two times increase. There are two reasons for this phenomenon. Firstly, this can be explained by a simple harmonic motion model following Hooke's law [22]:

$$\omega = \left(\frac{k}{m}\right)^{\frac{1}{2}} \quad (13)$$

where ω is the lattice vibration frequency, k is the stiffness coefficient, and m is the atomic weights. The atomic weights of Ge^{4+} and Ti^{4+} are 72.64 and 47.867, respectively, indicating that the introduction of Ge^{4+} can reduce the vibration frequency of the crystal lattice and makes it more stable.

Secondly, the improvement of thermal resistance can be linked to higher activation energy. The E_a of phosphors were calculated by following equation [41]:

$$\ln\left[\left(\frac{I_0}{I}\right) - 1\right] = -\frac{E_a}{kT} + c \quad (14)$$

where I is the luminescent intensity at T, I_0 is the luminescent intensity at indoor temperature, c and T stand for a constant and the Kelvin temperature, respectively. The value of k is the Boltzmann constant (8.62×10^{-5} eV). Fig. 9a represent the relationship between the 1/kT and ln[(I_0/I)-1] of $Li_2MgTi_{0.998-y}O_4$: $0.002Mn^{4+}$, yGe^{4+} (y = 0, 0.1) phosphors. The slopes of the two fitting lines are −0.254 and −0.386, so the E_{a1} and E_{a2} are 0.254 eV and 0.386 eV respectively. Meanwhile, Fig. 9b exhibits the configurational coordinate diagram for Mn^{4+} in $Li_2MgTi_{0.998-y}O_4$: $0.002Mn^{4+}$, yGe^{4+} phosphors. As described above, the excited electrons of $^4T_1$, $^2T_2$, and $^4T_2$ relax to ^2E through multiple non-radiative processes, and then a luminescence of 675 nm can be observed due to the $^2E \rightarrow {}^4A_2$ electronic transition. However, as the temperature increases, the excited electrons are able to return to $^4A_2$ through the intersection between $^4T_2$ and $^4A_2$, rather than through the radiative transition from ^2E to $^4A_2$. Therefore, the luminescence intensity of phosphors is quenched rapidly. The introduction of Ge^{4+} can reduce this additional non-radiative transition by increasing the energy barrier of E_a, keeping the excitation energy released through the normal radiative pathway.

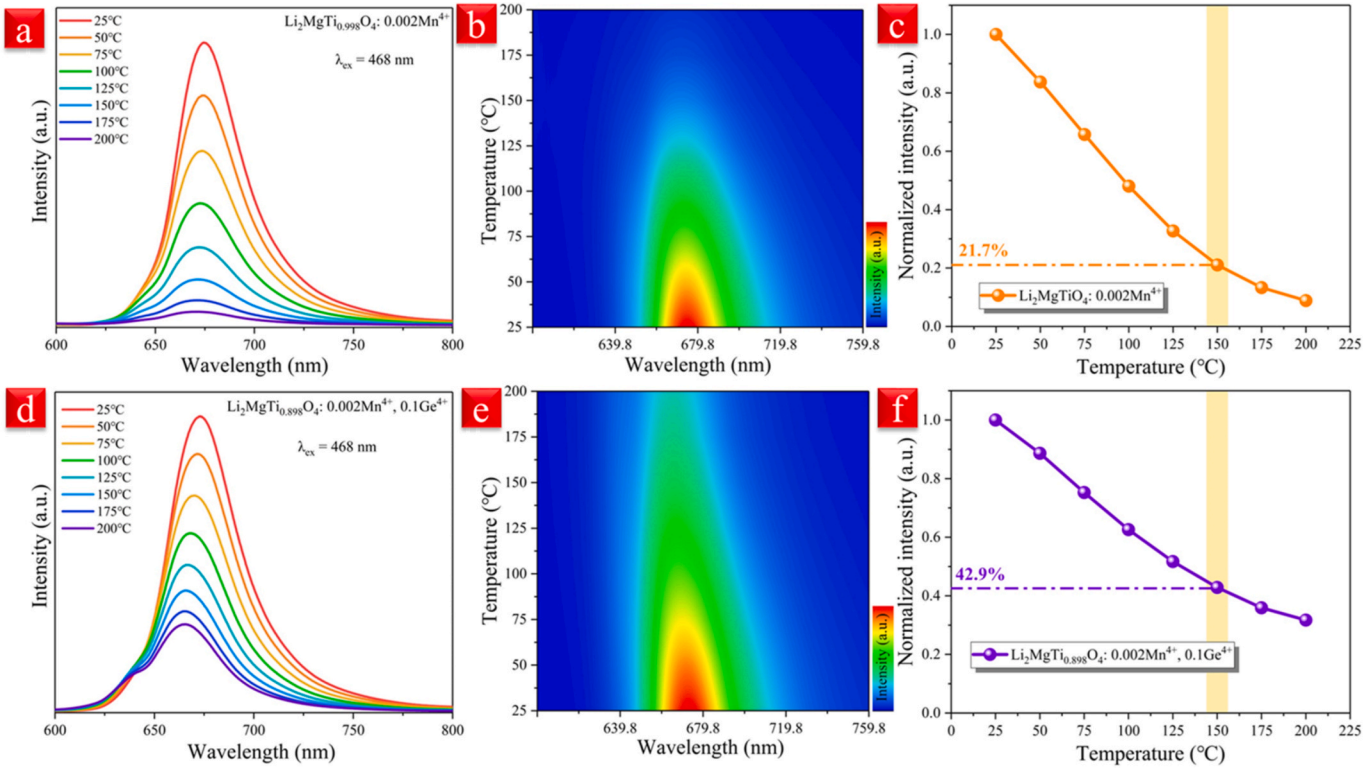

Fig. 8. (a–f) Temperature dependence of the emission intensity of $Li_2MgTi_{0.998}O_4$: $0.002Mn^{4+}$ and $Li_2MgTi_{0.898}O_4$: $0.002Mn^{4+}$, $0.1Ge^{4+}$.

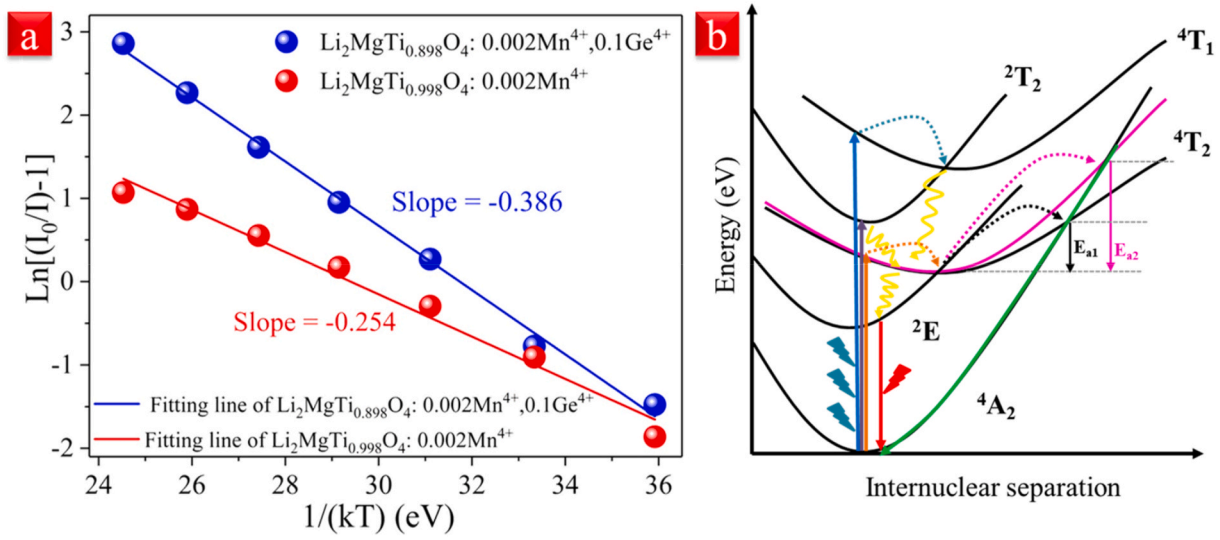

Fig. 9. (a) The relation between emission intensity and temperature of phosphor. (b) The configurational coordinate diagram for Mn^{4+} ions in $Li_2MgTi_{0.998-y}O_4$: $0.002Mn^{4+}$, yGe^{4+} phosphors.

3.4. EL spectra and CIE chromaticity coordinates

Six pc-LED were assembled with different contents of $Li_2MgTi_{0.898}O_4$: $0.002Mn^{4+}$, $0.1Ge^{4+}$ phosphors and 470 nm blue chips, showing different luminescence intensity at blue (470 nm) and red (675 nm) light (Fig. 10a and b). the CIE chromaticity coordinates of the LED devices were calculated as (0.1540, 0.0401), (0.1633, 0.0442), (0.2217, 0.0761), (0.2684, 0.1140), (0.3931, 0.1421) and (0.6766, 0.2667) as shown in Fig. 10c. The electroluminescence spectrum (Fig. 10d) matches well with the absorption spectrum of Chlorophyll A and B and the overlap ratios with P_R and P_{FR} were calculated to be 46.69% and 56.78% respectively (Fig. 10e and f), indicating that the $Li_2MgTi_{0.898}O_4$: $0.002Mn^{4+}$, $0.1Ge^{4+}$ phosphor has the potential applications in indoor plant cultivation.

4. Conclusion

In this work, $Li_2MgTi_{0.998-y}O_4$: $0.002Mn^{4+}$, yGe^{4+} ($y = 0$, 0.05, 0.1, 0.15, 0.2) red emitting phosphors have been synthesized via solid state reaction method. The XRD patterns show pure phase of Li_2MgTiO_4 can be formed when the concentration of Ge^{4+} is less than or equal to 0.1. Above that, the 2nd phase of Li_2MgTiO_4 starts to develop, impacting the emission intensity. When the concentration of Ge^{4+} reaches 0.1, the emission intensity increased by 152%, which was mainly caused by the

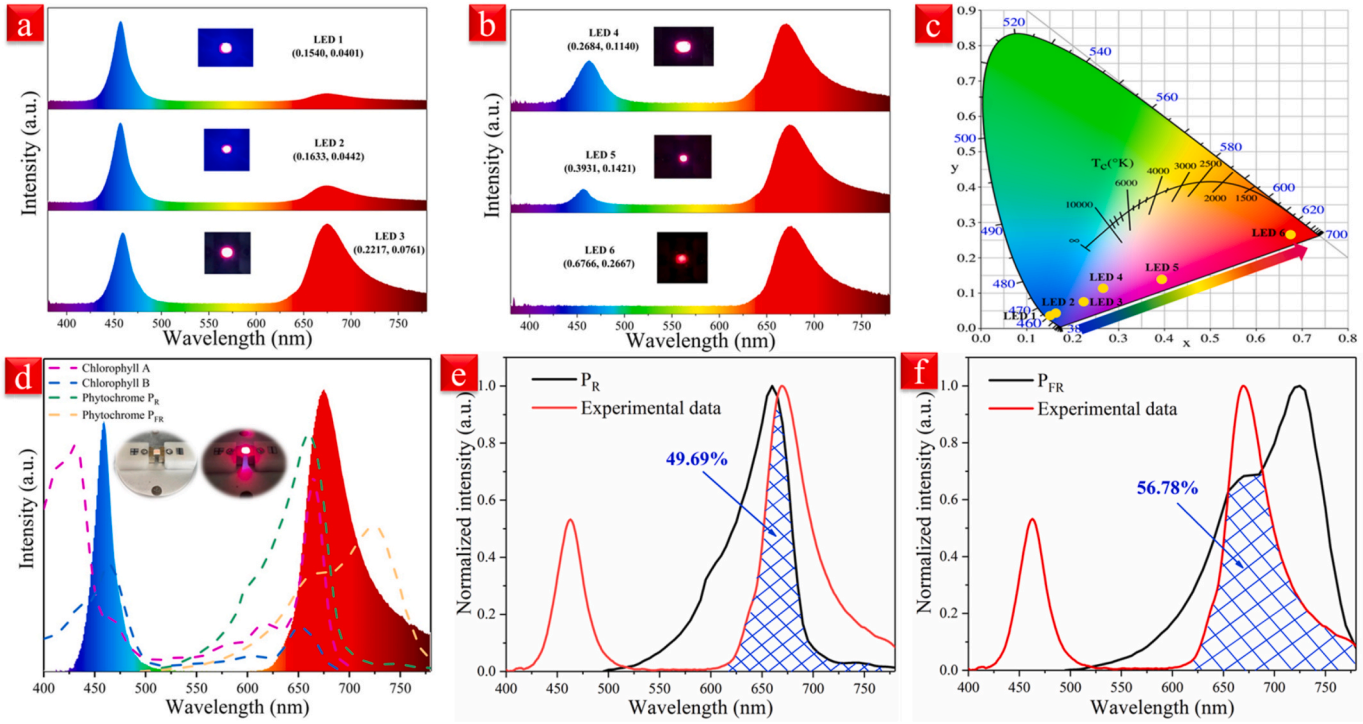

Fig. 10. (a) (b) EL spectra of the $Li_2MgTi_{0.898}O_4$: $0.002Mn^{4+}$, $0.1Ge^{4+}$ with different content, the insets are photos of the LED devices. (c) CIE chromaticity coordinates. (d) Comparison of the emission spectra and absorption curves of plant pigment, the insets are photos of the LED device. (e), (f) The overlap ratios with P_R and P_{FR}.

increased isolation degree of Mn^{4+}. The thermal resistance of the $Li_2MgTi_{0.898}O_4$: $0.002Mn^{4+}$, $0.1Ge^{4+}$ phosphor at 150 °C is 42.9%, which is 21.7% higher than that without doping. This result can be attributed to the reduced lattice vibrations and higher activation energy. The luminescence lifetime of the optimal phosphor is 0.406 ms. The IQY increases from 18.8% to 19.6%. Finally, the pc-LED devices were assembled with different contents of $Li_2MgTi_{0.898}O_4$: $0.002Mn^{4+}$, $0.1Ge^{4+}$ and 470 nm blue chips showed that the emission spectra matched well with the absorption regions, demonstrating the potential of the $Li_2MgTi_{0.898}O_4$: $0.002Mn^{4+}$, $0.1Ge^{4+}$ phosphor in indoor plant cultivation.

Declaration of competing interest

The authors declare that they have no known competing financial interests or personal relationships that could have appeared to influence the work reported in this paper.

Acknowledgements

The authors would like to gratefully acknowledge funds from National Natural Science Foundation of China (Grant No. 51974123), the Distinguished Youth Foundation of Hunan Province (Grant No. 2020JJ2018), Key R & D projects in Hunan Province (2020WK2016&2020SK2032), Hunan High Level Talent Gathering Project (2019RS1077&2020RC5007), the Natural Sciences Foundation of Hunan Agricultural University (19QN11), Hunan Provincial Key Laboratory of Crop Germplasm Innovation and Resource Utilization Science Foundation (19KFXM12), Changsha Science and technology plan (KH2005114), and the Scientific Research Fund of Hunan Provincial Education Department (19C0903).

References

[1] S. Demotes-Mainard, T. Peron, A. Corot, J. Bertheloot, J. Le Gourrierec, S. Pelleschi-Travier, L. Crespel, P. Morel, L. Huche-Thelier, R. Boumaza, A. Vian, V. Guerin, N. Leduc, S. Sakr, Plant responses to red and far-red lights, applications in horticulture, Environ. Exp. Bot. 121 (2016) 4–21, https://doi.org/10.1016/j.envexpbot.2015.05.010.

[2] J.M. Xiang, J.M. Zheng, Z.W. Zhou, H. Suo, X.Q. Zhao, X.J. Zhou, N.M. Zhang, M. S. Molokeev, C.F. Guo, Enhancement of red emission and site analysis in Eu^{2+} doped new-type structure $Ba_3CaK(PO_4)_3$ for plant growth white LEDs, Chem. Eng. J. 356 (2019) 236–244, https://doi.org/10.1016/j.cej.2018.09.036.

[3] Y. Zhong, S.J. Gai, M. Xia, S.M. Gu, Y.L. Zhang, X.B. Wu, J. Wang, N. Zhou, Z. Zhou, Enhancing quantum efficiency and tuning photoluminescence properties in far-red-emitting phosphor $Ca_{14}Ga_{10}Zn_6O_{35}$: Mn^{4+} based on chemical unit engineering, Chem. Eng. J. 374 (2019) 381–391, https://doi.org/10.1016/j.cej.2019.05.201.

[4] L. Shi, S. Wang, Y.J. Han, Z.X. Ji, D. Ma, Z.F. Mu, Z.Y. Mao, D.J. Wang, Z.W. Zhang, L. Liu, Sr_2LaSbO_6: Mn^{4+} far-red phosphor for plant cultivation: synthesis, luminescence properties and emission enhancement by Al^{3+} ions, J. Lumin. 221 (2020) 117091, https://doi.org/10.1016/j.jlumin.2020.117091.

[5] Z. Zhou, Y. Zhong, M. Xia, N. Zhou, B.F. Lei, J. Wang, F.F. Wu, Tunable dual emission of $Ca_3Al_4ZnO_{10}$: Bi^{3+}, Mn^{4+} via energy transfer for indoor plant growth lighting, J. Mater. Chem. C 6 (2018) 8914–8922, https://doi.org/10.1039/c8tc02792g.

[6] X.Y. Huang, H. Guo, Finding a novel highly efficient Mn^{4+}-activated $Ca_3La_2W_2O_{12}$ far-red emitting phosphor with excellent responsiveness to phytochrome P_{FR}: towards indoor plant cultivation application, Dyes Pigments 152 (2018) 36–42, https://doi.org/10.1016/j.dyepig.2018.01.022.

[7] S.Q. Fang, T.C. Lang, T. Han, M.S. Cai, S.X. Cao, L.L. Peng, B.T. Liu, Y. Zhong, A. N. Yakovlev, V.I. Korepanov, A novel efficient single-phase dual-emission phosphor with high resemblance to the photosynthetic spectrum of chlorophyll A and B, J. Mater. Chem. C 8 (2020) 6245–6253, https://doi.org/10.1039/d0tc00811g.

[8] Y. Zhong, Y. Zhou, C. Zhou, H.X. Chen, Z. Zhou, M.G. Brik, M. Xia, Two targets with one strategy: insights into the role of aluminum atoms on the luminescence properties and thermal stability in Mn^{4+}-doped calcium aluminozincate phosphor, J. Alloys Compd. 849 (2020) 156567, https://doi.org/10.1016/j.jallcom.2020.156567.

[9] G. Zhang, W.B. Chen, Y.A. Wang, X. Chen, Y.Y. Li, L. Zhao, Y.Q. Yang, Synthesis and luminescence properties of a novel deep red phosphor $Li_2ZnTi_3O_8$: Mn^{4+} for plant-cultivation, Spectrochim. Acta 240 (2020) 118567, https://doi.org/10.1016/j.saa.2020.118567.

[10] D. Singh, C. Basu, M. Meinhardt-Wollweber, B. Roth, LEDs for energy efficient greenhouse lighting, Renew. Sustain. Energy Rev. 49 (2015) 139–147, https://doi.org/10.1016/j.rser.2015.04.117.

[11] R.P. Cao, Z.H. Shi, G.J. Quan, T. Chen, S.L. Guo, Z.F. Hu, P. Liu, Preparation and luminescence properties of Li_2MgZrO_4 :Mn^{4+} red phosphor for plant growth, J. Lumin. 188 (2017) 577–581, https://doi.org/10.1016/j.jlumin.2017.05.002.

[12] L. Kong, Y.Y. Liu, L.P. Dong, L. Zhang, L. Qiao, W.S. Wang, H.P. You, Enhanced red luminescence in $CaAl_{12}O_{19}$: Mn^{4+} via doping Ga^{3+} for plant growth lighting, Dalton Trans. 49 (2020) 1947–1954, https://doi.org/10.1039/C9DT04086B.

[13] Z. Zhou, N. Zhou, X.Y. Lu, M.T. Kate, D. Valdesueiro, J. Ruud van Ommen, H. T. Hintzen, Performance improvement by alumina coatings on $Y_3Al_5O_{12}$: Ce^{3+} phosphor powder deposited using atomic layer deposition in a fluidized bed reactor, RSC Adv. 6 (2016) 76454–76462, https://doi.org/10.1039/C6RA12983H.

[14] X.J. Zhang, J.B. Yu, J. Wang, B.F. Lei, Y.L. Liu, Y.J. Cho, R.J. Xie, H.W. Zhang, Y. R. Li, Z.F. Tian, Y. Li, Q. Su, All-inorganic light convertor based on phosphor-in-glass engineering for next-generation modular high-brightness white LEDs/LDs, ACS Photonics 4 (2017) 986–995, https://doi.org/10.1021/acsphotonics.7b00049.

[15] L. Wang, R.J. Xie, Y.Q. Li, X.J. Wang, C.G. Ma, D. Luo, T. Takeda, Y.T. Tsai, R. S. Liu, N. Hirosaki, $Ca_{1-x}Li_xAl_{1-x}Si_{1+x}N_3$: Eu^{2+} solid solutions as broadband, color-tunable and thermally robust red phosphors for superior color rendition white light-emitting diodes, Light Sci. Appl. 5 (2016), https://doi.org/10.1038/lsa.2016.155 e16155–e16155.

[16] Y.T. Tsai, C.Y. Chiang, W. Zhou, J.F. Lee, H.S. Sheu, R.S. Liu, Structural ordering and charge variation induced by cation substitution in (Sr,Ca)$AlSiN_3$: Eu Phosphor, J. Am. Chem. Soc. 137 (2015) 8936–8939, https://doi.org/10.1021/jacs.5b06080.

[17] S.L. Chung, W.C. Chou, J. Heo, Combustion synthesis of $Ca_2Si_5N_8$: Eu^{2+} phosphors and their luminescent properties, J. Am. Ceram. Soc. 96 (2013) 2086–2092, https://doi.org/10.1111/jace.12369.

[18] M. Zeuner, P.J. Schmidt, W. Schnick, One-pot synthesis of single-source precursors for nanocrystalline LED phosphors $M_2Si_5N_8$: Eu^{2+} (M = Sr, Ba), Chem. Mater. 21 (2009) 2467–2473, https://doi.org/10.1021/cm900341f.

[19] H.M. Zhu, C.C. Lin, W.Q. Luo, S.T. Shu, Z.G. Liu, Y.S. Liu, J.T. Kong, E. Ma, Y. G. Cao, R.S. Liu, X.Y. Chen, Highly efficient non-rare-earth red emitting phosphor for warm white light-emitting diodes, Nat. Commun. 5 (2014) 4312, https://doi.org/10.1038/ncomms5312.

[20] Y.Y. Zhou, C.K. Yu, E. Song, Y.H. Wang, H. Ming, Z.G. Xia, Q.Y. Zhang, Three birds with one stone: K_2SiF_6: Mn^{4+} single crystal phosphors for high-power and laser-driven lighting, Adv. Opt. Mater. 8 (2020) 202000976, https://doi.org/10.1002/ADOM. 202000976.

[21] Y.J. Zheng, H.M. Zhang, H.R. Zhang, Z.G. Xia, Y.L. Liu, M.S. Molokeev, B.F. Lei, Co-substitution in $Ca_{1-x}Y_xAl_{12-x}Mg_xO_{19}$ phosphors: local structure evolution, photoluminescence tuning and application for plant growth LEDs, J. Mater. Chem. C 6 (2018) 4217–4224, https://doi.org/10.1039/c8tc00165k.

[22] S.Q. Fang, T.C. Lang, T. Han, J.Y. Wang, J.Y. Yang, S.X. Cao, L.L. Peng, B.T. Liu, A. N. Yakovlev, V.I. Korepanov, Zero-thermal-quenching of Mn^{4+} far-red-emitting in $LaAlO_3$ perovskite phosphor via energy compensation of electrons' traps, Chem. Eng. J. 389 (2020) 124297, https://doi.org/10.1016/j.cej.2020.124297.

[23] S.M. Gu, M. Xia, C. Zhou, Z.H. Kong, M.S. Molokeev, L. Liu, W.Y. Wong, Z. Zhou, Red shift properties, crystal field theory and nephelauxetic effect on Mn^{4+}-doped $SrMgAl_{10-y}Ga_yO_{17}$ red phosphor for plant growth LED light, Chem. Eng. J. 396 (2020) 125208, https://doi.org/10.1016/j.cej.2020.125208.

[24] Y.H. Jin, Y.H. Hu, H.Y. Wu, H. Duan, L. Chen, Y.R. Fu, G.F. Ju, Z.F. Mu, M. He, A deep red phosphor Li_2MgTiO_4: Mn^{4+} exhibiting abnormal emission: potential application as color converter for warm w-LEDs, Chem. Eng. J. 288 (2016) 596–607, https://doi.org/10.1016/j.cej.2015.12.027.

[25] L.F. Nien, C.H. Chiang, H.H. Nien, S.Y. Chu, Effects of HfO_2 dopant on characteristics of Li_2MgTiO_4-based red phosphors: thermal stability, photoluminescence intensity and quantum efficiency improvement, Ceram. Int. 44 (2018) 15428–15431, https://doi.org/10.1016/j.ceramint.2018.05.196.

[26] Y.L. Zhang, Y.D. Huang, M.H. Li, C. Liang, H.F. Zhu, Y. Zhong, N. Yang, Z. Zhou, M. Xia, Tuning the luminescence properties of Mn^{4+}-activated $CaYAlO_4$ phosphor by co-doping cations for indoor plant cultivation, J. Am. Ceram. Soc. 103 (2020) 4373–4383, https://doi.org/10.1111/JACE.17111.

[27] Y. Zhong, N. Zhou, M. Xia, Y. Zhou, H.X. Chen, Z. Zhou, Synthesis and photoluminescence properties of novel red-emitting phosphor $SrAl_3BO_7$:Mn^{4+} with enhanced emission by Mg^{2+}/Zn^{2+}/Ca^{2+} incorporation for plant growth LED lighting, Ceram. Int. 45 (2019) 23528–23539, https://doi.org/10.1016/j.ceramint.2019.08.062.

[28] R.P. Cao, X.Y. Cheng, F.T. Zhang, L. Su, T. Chen, H. Ao, X.G. Yu, W. Ruan, Enhanced luminescence properties of $MgTO_3$: Mn^{4+} red-emitting phosphor by adding Ge^{4+} ion and H_3BO_3, J. Mater. Sci. Mater. Electron. 29 (2018) 13005–13010, https://doi.org/10.1007/s10854-018-9421-5.

[29] L.L. Peng, W.B. Chen, S.X. Cao, B.T. Liu, T. Han, Z. Lei, C. Zhao, F. Li, X.M. Li, Enhanced photoluminescence and thermal properties of size mismatch in $Mg_2Ti_xGe_{1-x}O_4$:Mn^{4+} deep-red phosphors, J. Mater. Chem. C 7 (2019) 2345–2552, https://doi.org/10.1039/c8tc05743e.

[30] R.P Cao, D. Ceng, X.G. Yu, S.L. Guo, Y.F. Wen, G.T. Zheng, Synthesis and luminescence properties of novel deep red emitting phosphors Li_2MgGeO_4: Mn^{4+}, Funct. Mater. Lett. 8 (2015) 1550046, https://doi.org/10.1142/S1793604715500460.

[31] H.F. Zhu, S.Q. Feng, Z.H. Kong, X. Huang, L. PenG, J. Wang, W.Y. Wong, Z. Zhou, M. Xia, Bi^{3+} occupancy rearrangement in $K_{2-x}A_xMgGeO_4$ phosphor to achieve ultra-broad-band white emission based on alkali metal substitution engineering, Appl. Surf. Sci. 563 (2021) 150252.

[32] M. Xia, S.M. Gu, C. Zhou, L.H. Liu, Y. Zhong, Y.L. Zhang, Z. Zhou, Enhanced photoluminescence and energy transfer performance of $Y_3Al_4GaO_{12}$: Mn^{4+}, Dy^{3+} phosphors for plant growth LED lights, RSC Adv. 9 (2019) 9244–9252, https://doi.org/10.1039/C9RA00700H.

[33] X.B. Wu, L.H. Liu, M. Xia, S.X. Huang, Y. Zhou, W. Hu, Z. Zhou, N. Zhou, Enhance the luminescence properties of $Ca_{14}Al_{10}Zn_6O_{35}$: Ti^{4+} phosphor via cation vacancies engineering of Ca^{2+} and Zn^{2+}, Ceram. Int. 45 (2019) 9977–9985, https://doi.org/10.1016/j.ceramint.2019.02.041.

[34] Z.X. Wang, H. Lin, D.W. Zhang, Y.M. Shen, Y. Li, R.J. Hong, C.X. Tao, Z.X. Han, L. Chen, S.M. Zhou, Deep-red emitting Mg_2TiO_4: Mn^{4+} phosphor ceramics for plant lighting, J. Adv. Ceram. 10 (2020) 88–97, https://doi.org/10.1007/s40145-020-0421-6.

[35] P.X. Gao, P. Dong, Z.Y. Zhou, Q. Li, H.H. Li, Z. Zhou, M. Xia, P.H. Zhang, Enhanced luminescence and energy transfer performance of double perovskite structure Gd_2MgTiO_6: Bi^{3+}, Mn^{4+} phosphor for indoor plant growth LED lighting, Ceram. Int. 47 (2021) 16588–16596, https://doi.org/10.1016/j.ceramint.2021.02.230.

[36] D.Q. Trung, N. Tu, N.V. Quang, M.T. Tran, N.V. Du, P.T. Huy, Non-rare-earth dual green and red-emitting Mn-doped $ZnAl_2O_4$ phosphors for potential application in plan-growth LEDs, J. Alloys Compd. 845 (2020) 156326, https://doi.org/10.1016/j.jallcom.2020.156326.

[37] Y.J. Han, S. Wang, H. Liu, L. Shi, J.Y. Zhang, Z.N. Zhang, Z.Y. Mao, D.J. Wang, Z. F. Mu, Z.W. Zhang, Y. Zhao, Synthesis and luminescent properties of a novel deep-red phosphor Sr_2GdNbO_6: Mn^{4+} for indoor plant growth lighting, J. Lumin. 220 (2020) 116968, https://doi.org/10.1016/j.jlumin.2019.116968.

[38] S.J. Gai, H.F. Zhu, P.X. Gao, C. Zhou, Z.H. Kong, M.S. Molokeev, Z.Y. Qi, Z. Zhou, M. Xia, Structure analysis, tuning photoluminescence and enhancing thermal stability on Mn^{4+}-doped $La_{2-x}Y_xMgTiO_6$ red phosphor for agricultural lighting, Ceram. Int. 46 (2020) 20173–20182, https://doi.org/10.1016/j.ceramint.2020.05.095.

[39] B. Wang, H. Lin, F. Huang, J. Xu, H. Chen, Z.B. Lin, Y.S. Wang, Non-Rare-Earth $BaMgAl_{10-2x}O_{17}$: xMn^{4+}, xMg^{2+}: a narrow-band red phosphor for use as a high-power warm w-LED, Chem. Mater. 28 (2016) 3515–3524, https://doi.org/10.1021/acs.chemmater.6b01303.

[40] B. Wang, H. Lin, J. Xu, H. Chen, Y.S. Wang, $CaMg_2Al_{16}O_{27}$: Mn^{4+}-based red phosphor: a potential color converter for high-powered warm W-LED, ACS Appl. Mater. Interfaces 6 (2014) 22905–22913, https://doi.org/10.1021/am507316b.

[41] F.G. Zhou, M. Gao, Y.R. Shi, Z.W. Li, G. Zhu, S.Y. Xin, C. Wang, Structure identification and strongly enhanced luminescence of $Sr_9Y_2(WO_6)_4$: Mn^{4+} phosphors by co-doping Mg^{2+} ions for plant growth LEDs, J. Lumin. 223 (2020) 117235, https://doi.org/10.1016/j.jlumin.2020.117235.